PCCP

PAPER

View Article Online
View Journal | View Issue

Cite this: *Phys. Chem. Chem. Phys.*, 2018, **20**, 24329

Bexarotene cannot reduce amyloid beta plaques through inhibition of production of amyloid beta peptides: *in silico* and *in vitro* study†

Huy Dinh Quoc Pham,‡[ab] Nguyen Quoc Thai,‡[bcd] Zuzana Bednarikova,[e] Huynh Quang Linh,[c] Zuzana Gazova*[e] and Mai Suan Li ‡*[a]

Received 4th January 2018,
Accepted 29th August 2018

DOI: 10.1039/c8cp00049b

rsc.li/pccp

Recently, it has been reported that anti-cancer drug bexarotene can remarkably destroy amyloid beta (Aβ) plaques in mouse models suggesting therapeutic potential for Alzheimer's disease. However, the effect of bexarotene on clearance of plaques has not been seen in some mouse models. One of the possible mechanisms explaining this phenomenon is that bexarotene levels up expression of apolipoprotein 4 (ApoE4) leading to intracellular clearance of Aβ peptide. Therefore, an interesting question emerges of whether bexarotene can destroy Aβ plaques by direct interaction with them or by preventing production of Aβ peptides. In our previous work we have shown that bexarotene cannot clear amyloid aggregates due to their weak interaction using *in silico* and *in vitro* experiments. Here we explore the possibility of inhibiting Aβ production through bexarotene binding to β-secretase which can cleave Aβ peptides from amyloid precursor protein. Using the molecular mechanics-Poisson–Boltzmann surface area method and all-atom simulations we have shown that bexarotene has a very low binding affinity to β-secretase. This result has been also confirmed by our *in vitro* experiment implying that bexarotene cannot clear amyloid plaques through inhibition of Aβ production. We have also shown that bexarotene tightly binds to both peroxisome proliferator-activated receptor γ (PPAR-γ) and retinoid X receptors (RXRs). Thus, our result does not contradict the hypothesis that the reduction of Aβ plaques occurs due to bexarotene-induced overexpression of ApoE4.

Introduction

Alzheimer's disease (AD) is a devastating and so far incurable neurodegenerative disease mainly occurring late in life. The prevalence of AD is proposed to be 114 million patients by 2020. Therefore, Alzheimer's disease poses a great financial, medical and social burden to society. Despite decades of research the origin and pathogenesis of this progressive disease remain largely unclear and none of the clinically tested drugs have been proved to be clinically effective.

According to the amyloid cascade hypothesis,[1,2] the pathogenesis of AD is associated with progressive extracellular accumulation of amyloid oligomers and plaques that consist of Aβ peptides formed by sequential processing of amyloid precursor protein (APP). APP is a type I transmembrane protein that is produced at high concentrations in neurons and has a rapid metabolism.[3] APP can be processed by different pathways which lead to generation of Aβ peptides or not. The cleavage of APP by α-secretase causes release of soluble and most likely neuroprotective sAPPα.[4]

The generation of Aβ peptides starts by cleavage of APP by β-secretase. Several studies have identified BACE-1 (transmembrane aspartic protease) as the primary β-secretase. Changes in activity or levels of BACE-1 affect cleavage of APP at the β-site locations. It has been shown that BACE-1 deficiency in AD mice reduces neuronal loss, cholinergic dysfunction and memory deficits which were in correlation with a significant reduction in amyloid β peptide concentration.[5] Several studies have found that the concentration and activity of BACE-1 are increased in parts of

[a] *Institute of Physics, Polish Academy of Sciences, Al. Lotnikow 32/46, 02-668 Warsaw, Poland. E-mail: masli@ifpan.edu.pl*
[b] *Institute for Computational Science and Technology, Quang Trung Software City, Tan Chanh Hiep Ward, District 12, Ho Chi Minh City, Vietnam*
[c] *Biomedical Engineering Department, University of Technology, VNU HCM 268, Ly Thuong Kiet Str., Distr. 10, Ho Chi Minh City, Vietnam*
[d] *Division of Theoretical Physics, Dong Thap University, 783 Pham Huu Lau Str., Ward 6, Cao Lanh City, Dong Thap, Vietnam*
[e] *Department of Biophysics, Institute of Experimental Physics, Slovak Academy of Sciences, Watsonova 47, 040 01 Kosice, Slovakia. E-mail: gazova@saske.sk*

† Electronic supplementary information (ESI) available: Optimized structure and parameters used for simulation of bexarotene; the binding free energies of bexarotene to PPAR-γ, RXR-α, and β-secretase in four MD runs; and the time dependence of the RMSD and interaction energy of the complexes of bexarotene with RXR-α, and β-secretase. See DOI: 10.1039/c8cp00049b

‡ Contributed equally.

the brain affected by AD.[6] So, it might seem that targeting BACE-1 is a good approach for a treatment of AD. However, inhibition of BACE-1 activity or a lack of enzyme in mice models resulted in altered neurological and hyperactive behaviors or death of BACE-1 KO mice in the first weeks after birth.[7] Upon BACE-1 cleavage, the APP C-terminal fragment is further cleaved by γ-secretase to generate Aβ peptides of 36–43 amino acids and the APP intracellular domain.[8] The most abundant forms of Aβ peptides are $A\beta_{1-40}$ or $A\beta_{1-42}$ with 40 and 42 amino acids, respectively.

The clearance of soluble forms of Aβ peptides is facilitated from brain interstitial fluid by apolipoprotein E (ApoE). ApoE is a cholesterol and phospholipids transporting protein that scaffolds high-density lipoprotein particle formation. The ApoE-lipoprotein particles can interact with soluble Aβ peptides stimulating their clearance from the brain.[9] ApoE expression is regulated *via* the action of nuclear receptor PPAR-γ (peroxisome proliferator-activated receptor γ) and the liver X receptor (LXR) jointly with the retinoid X receptor (RXR), representing a target for pharmacological modulation of complex levels.

Bexarotene is a RXR agonist and has been used as an anti-cancer agent for the treatment of cutaneous T cell lymphoma.[10] Recently, Cramer *et al.*[11] have reported that bexarotene shows a great efficacy in reducing Aβ plaques in mice models of AD. They proposed that bexarotene is binding and activating the PPAR-γ, LXR and RXR receptors resulting in increase of the ApoE expression and its association with lipoproteins leading to enhancement of the Aβ clearance mechanisms from the brain. Increased clearance of soluble Aβ peptides from the brain and interstitial fluid was associated with improvement in memory and cognitive activity in *in vivo* models.[11,12] It was a very promising result but the strong Aβ clearance was reproducible in some mouse models but not in all of them[13–16] making the situation unclear. Dickey *et al.*[17] tested the effect of bexarotene in various *in vitro* cellular models of Huntington's disease (HD) and observed robust neuroprotection which also involved PPAR-δ activation. They considered PPARδ activation based on its formation of permissive heterodimers with RXR and found that bexarotene treatment counters mutant huntingtin toxicity both *in vitro* and *in vivo* in HD.

The other ongoing controversy is the effect of bexarotene on humans. Bexarotene is currently in clinical trials in AD. It was previously shown that bexarotene readily crosses the blood–brain barrier in mice models; it is not so efficient in the case of crossing the BBB in healthy humans. This indicates that therapeutic responses observed in patients may stem from the peripheral benefits of RXR and PPAR activation or from alteration of BBB function in human patients.[9]

From the theoretical point of view the role of bexarotene in AD pathways remains largely unknown. Fantini *et al.*[18] have proposed that bexarotene competes with cholesterol for binding to Aβ and inhibits its aggregation as a result. Wajid *et al.*[19] using molecular docking have predicted therapeutic potential of bexarotene in Alzheimer's disease as it has respectable binding energy patterns for β-secretase and presenilin-1. In our previous work[20] we explored whether bexarotene can directly destroy $A\beta_{42}$ fibrils and how it influences the fibril growth process using *in vitro* and *in silico* methods. Our *in vitro* experiments disclosed that bexarotene does not reverse the fibrillation but it can delay the self-assembly process. The prolongation of the lag phase by bexarotene has been also reported by Habchi *et al.*[21,22] Combining the docking and molecular mechanics-Poisson–Boltzmann surface area (MM-PBSA) methods we have shown that bexarotene is weakly bound to $A\beta_{42}$ fibrils.[20] These results suggested that bexarotene does not reduce the amount of $A\beta_{42}$ fibrils. For the first time we have described the molecular mechanisms of the prolongation of the lag phase. Namely, by all-atom MD simulations in explicit water we have shown that upon bexarotene binding the β-sheet content in the monomeric state of the Aβ peptide gets reduced leading to an increase of the fibril formation time.[20] From this prospect, bexarotene may delay the fibril formation but the clearance of Aβ plaques from the brain is not due to its direct interaction with Aβ.

In this study, using molecular simulation and *in vitro* experiment we ask the following questions: (1) is the binding of bexarotene to PPAR-γ and retinoid X receptors (RXRs) strong enough to enhance the ApoE4 expression? (2) Can bexarotene interfere with Aβ production from APP through strong binding to the β-secretase? Combining the docking and molecular mechanics-Poisson–Boltzmann surface area (MM-PBSA)[23] methods we have shown that bexarotene strongly binds to both PPAR-γ and RXRs supporting the hypothesis[11] that Aβ clearance from the brain may be due to ApoE overexpression. Our *in silico* experiments have revealed that bexarotene is weakly bound to β-secretase and this result was also confirmed by *in vitro* experiments. Thus, our study suggests that bexarotene cannot prevent Aβ production through inhibiting the activity of β-secretase.

Material and methods

Structure of bexarotene

$C_{24}H_{28}O_2$ is the chemical formula of bexarotene, and the 2D structure is shown in Fig. 1A. For molecular simulation, using GaussView5, the 3D structure of bexarotene was first built, and then optimized by the GAUSSIAN09 package.[24] The method used to optimize the structure of bexarotene was Hartree–Fock[25] with the basis set 6-31G*. The optimized structure is shown in Fig. S1 in ESI.† Restrained electrostatic potential (RESP) charge was calculated by the Merz–Singh–Kollman scheme,[26,27] based on the optimized structure. Atomic names, types, and charges of bexarotene are given in Table S1 (ESI†). For those who wish to carry out simulation of bexarotene, we provide ESI† bexarotene_frcmod.docx that contains parameters of all bonds and angles.

Structures of three targets

The atomic structure of nuclear receptor peroxisome proliferator-activated receptor γ (PPAR-γ) was retrieved from PDB (PDB ID: 4EMA,[28] Fig. 1B). For retinoic X receptors the PDB structure of 4K6I was used since it is known that bexarotene binds to the RXR-α isoform[29] (Fig. 1C). For simulation of bexarotene

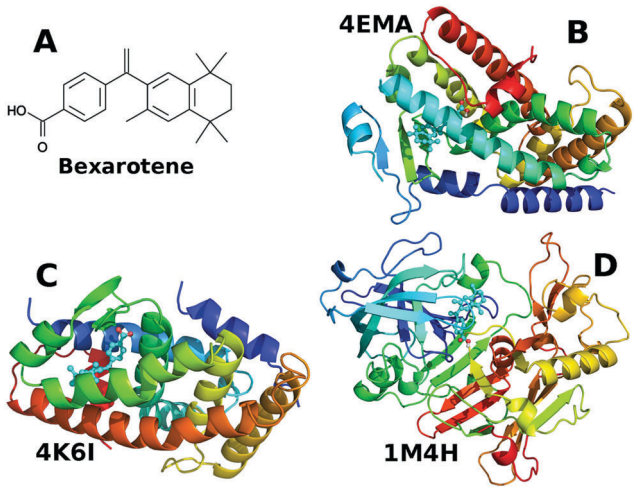

Fig. 1 (A) 2D structure of bexarotene. The PDB structures of PPAR-γ (B), RXR-α (C), and β-secretase (D). The pose of bexarotene in complex with targets was obtained in the best docking mode, except for the PPAR-γ where the holo-structure was taken from PDB.

binding to β-secretase we employed the PDB structure 1M4H[30] (Fig. 1D). The binding sites of all here mentioned targets are known from experiment.

Docking method

The position of bexarotene in the binding site of RXR is available from the PDB structure 4K6I[29] (Fig. 1C). To dock bexarotene to the binding site of PPAR-γ, β-secretase and RXR as a single target case, we have prepared a PDBQT file using AutodockTools 1.5.4.[31] The docking simulation has been carried out by Autodock Vina.[32] To achieve reliable results in the global search we set the exhaustiveness parameter equal to 400. In docking simulation the receptor dynamics was omitted. The scoring function is the binding (lowest) energy ΔE_{bind} obtained in the best docking mode.

Molecular dynamic (MD) simulation

The MD simulation was performed using the AMBER force field 99SB[33] implemented in the Amber11 package[33,34] combined with water model TIP3P.[35] The most suitable for the AMBER force field[36,37] has been the TIP3 model. The lowest energy structures, obtained by the docking method for target-bexarotene complexes, were utilized as initial structures for MD runs, except the RXR-α case, where the PDB structure was used. The leap-frog algorithm[38] was employed to solve the corresponding Langevin equations with time step Δt = 2 fs. By the SHAKE algorithm[39] the length constraint on bonds associated with a hydrogen atom was imposed. The temperature was maintained by the Langevin thermostat[40] having a frequency of collision equal to 2 ps^{-1}. For calculation of van der Waals (vdW) forces a cutoff of 1.4 nm was adopted, while the particle mesh Ewald (PME) summation method[41] was employed to compute the electrostatic energy. Every 10 fs we updated the pair-list for long-range interactions using a cutoff of 1.0 nm. The production runs were performed in the *NPT* mode. All simulations were performed at 300 K.

MM-PBSA method

According to this method[23] the binding free energy ΔG_{bind} has the following terms (more details on this method may be found elsewhere[42–44]):

$$\Delta G_{\text{bind}} = \Delta E_{\text{elec}} + \Delta E_{\text{vdW}} + \Delta G_{\text{sur}} + \Delta G_{\text{PB}} - T\Delta S, \quad (1)$$

where ΔE_{elec} and ΔE_{vdW} are electrostatic and van der Waals (vdW) interaction energies. ΔG_{PB} and ΔG_{sur} are polar and non-polar solvation energies. The entropy change ΔS was computed in the normal mode approximation.[45]

Tools and measures used for data analysis

RMSD (root mean square deviation) is defined as the deviation of the receptor backbone from its starting structure. A hydrogen bond (HB) was formed providing the distance between donor D and acceptor A is <3.5 Å, the H–A distance is <2.7 Å and the D–H–A angle is >135 degrees. A non-bonded contact (NBC) is defined as contact between atom C or O of the ligand and an atom of the protein molecule when they are within a distance of 3.9 Å. HBs and NBCs were analyzed by using LigPlot++version 1.44.[46]

Inhibition of β-secretase activity by bexarotene

The inhibitory activity of bexarotene on β-secretase was studied using a β-secretase (BACE-1) FRET Assay Kit (Pan Vera's, WI, USA). The stock solution of bexarotene in DMSO was serially diluted to a final concentration ranging from 100 pM to 1 mM (DMSO content in the reaction is $<2\%$) and added to the mixture containing 50 mM sodium acetate buffer, 250 nM BACE-1 substrate (rhodamine – EVNLDAEFK-Quencher) and 10 miliunits BACE-1 enzyme with a final pH value of ~ 6. The reaction was stopped after 90 min incubation at room temperature. Rhodamine fluorescence was monitored using 96-well half area microplates (Corning, NY, USA) on a Synergy Mx spectrofluorometer with excitation wavelength λ = 545 nm and emission recorded at 585 nm. The excitation and emission bandwidth was set at 13.5 nm. Error bars represent the standard deviation from average values of three independent measurements.

Results and discussion

After Cramer *et al.*[11] published their work, several groups put in great effort to understand the possible effect of bexarotene on AD. However, it is not clear which mechanisms lead to Aβ clearance associated with improvement in memory and cognitive activity in *in vivo* models upon binding bexarotene.[11,12] The direct effect of bexarotene on the formation or reversion of Aβ amyloid aggregates was not observed.[20] There is evidence that the activation of PPAR-γ and RXR receptors, which results in an increase of the ApoE concentration, leads to enhancement of the Aβ clearance mechanisms. The other possibility is the decrease of Aβ production from amyloid precursor protein (APP) through inhibition of β-secretase activity. Therefore, our study is focused on the interaction of bexarotene with PPAR-γ, RXR receptors and β-secretase with the aim to get better understanding of the effect of this small molecule in AD.

Docking results

Docking to the PBD structures. As mentioned above, the structures obtained in the best docking mode for bexarotene complexed with PPAR-γ, RXR and β-secretase are shown in Fig. 1. RXR belong to a superfamily of ETFs (eukaryotic transcription factors) and have 3 different isoforms α, β, and γ that form heterodimers with other nuclear receptors including PAR, RAR (retinoid acid receptor), LXR (liver X receptor), FXR (farnesoid X receptor), and TR (thyroid hormone receptor) as coregulators.[47] It is known that bexarotene binds to RXR-α; therefore, for our study we have used this isoform. The binding energy (ΔE_{bind}), and number of HBs and NBCs of bexarotene with all three targets were computed and data obtained in the best docking mode are presented in Table 1. Because bexarotene contains only two oxygen atoms, the HB networks are rather poor for all systems as it is evident from Fig. 2 where the HBs are highlighted by a green color. There is no HB between bexarotene and receptor PPAR-γ (Fig. 2A), while bexarotene forms 2 HBs with both RXR-α and β-secretase (Fig. 2B and C). The non-bonding contact networks of bexarotene in complex with the studied targets are also shown in Fig. 2.

Table 1 Binding energy ΔE_{bind} of bexarotene to PPAR-γ, RXR-α and β-secretase in the best docking mode. For RXR-α the result was obtained using the PDB holo structure. The numbers of hydrogen bonds (HBs) and non-bonded contacts (NBCs) between bexarotene and different targets are also shown

Complex	Hydrogen bonds	Non-bonded contacts	ΔE_{bind} (kcal mol^{-1})
PPAR-γ	0	12	−8.4
RXR-α	2	13	−12.6
β-Secretase	2	13	−9.1

Bexarotene has 12 non-bonded contacts with PPAR-γ. The same number of NBCs (13) was determined for bexarotene in complex with RXR-α and β-secretase. Overall, the binding energy ΔE_{bind} correlates with the number of HBs and NBCs (Table 1). The weakest binding affinity to PPAR-γ (ΔE_{bind} = −8.4 kcal mol^{-1}) is consistent with the smallest number of HBs (HB = 0) and NBCs (NBC = 12). In the case of the RXR-α + bexarotene complex the lowest binding energy (ΔE_{bind} = −12.6 kcal mol^{-1}) corresponds to the strongest HB and NBC networks (2 HBs and 13 NBCs). Having the same number of NBCs and HBs, the β-secretase + bexarotene complex however has the lower binding energy (Table 1). However, with ΔE_{bind} = −9.1 kcal mol^{-1}, our result is in reasonable agreement with Wajid *et al.*,[19] who demonstrated that bexarotene displays a respectable binding affinity to β-secretase using molecular docking. Based on the estimation of ΔE_{bind} the docking method predicts that bexarotene strongly binds to RXR-α (Table 1). However, as shown below by the more accurate MM-PBSA method, bexarotene has a very high binding affinity to both RXR-α and PPAR-γ, while the poor binding to β-secretase is confirmed. The main difference between the results obtained by docking and MD simulations is due to the fact that the receptor in the docking is rigid.

Docking to a set of equilibrium structures. One of the drawbacks of the docking method is that the dynamics of the receptor are neglected. In order to partially cure this problem we docked bexarotene to hundreds of receptor structures obtained at

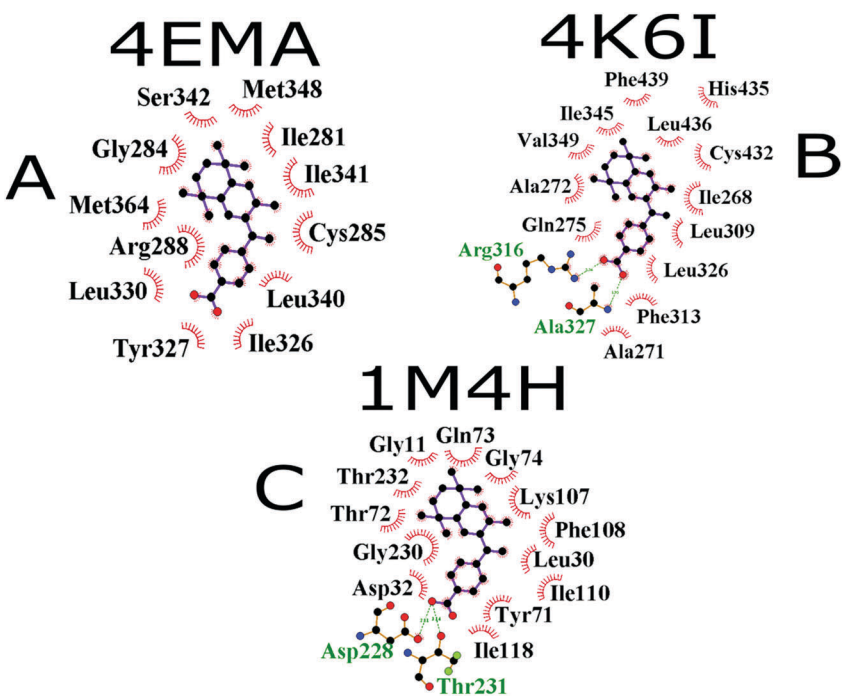

Fig. 2 Hydrogen bond (HB) (green line) and non-bonded contact (NBC) (represented by an arc with spokes radiating towards the ligand atoms they contact) networks of bexarotene in complex with PPAR-γ (A), RXR-α (B), and β-secretase (C). There are no HBs between bexarotene and PPAR-γ. Bexarotene forms 2 HBs with both RXR-α and β-secretase. Bexarotene has 12, 13, and 13 non-bonded contacts with PPAR-γ, RXR-α and β-secretase, respectively. The plots were prepared using LigPlot++version 1.44.

Table 2 Binding free energy ΔG_{bind} (kcal mol^{-1}) of bexarotene to PPAR-γ, RXR-α and β-secretase. The results were obtained by the MM-PBSA method

Targets	ΔE_{vdw}	ΔE_{ele}	ΔG_{PB}	ΔG_{sur}	$-T\Delta S$	ΔG_{bind}
PPAR-γ	−49.8 ± 0.9	−16.5 ± 2.3	34.6 ± 2.9	−4.6 ± 0.1	20.1 ± 1.4	−16.2 ± 1.8
RXR-α	−53.6 ± 1.5	−17.6 ± 2.3	38.7 ± 3.6	−4.5 ± 0.1	20.1 ± 1.4	−16.9 ± 3.0
β-Secretase	−26.5 ± 8.8	−10.3 ± 6.9	24.4 ± 10.9	−3.1 ± 0.9	14.9 ± 3.8	−0.56 ± 6.2

equilibrium in the MD simulation (see below). For the ten lowest binding energies of PPAR-γ and RXR-α bexarotene is located at the same position (Fig. 1). Therefore the MD simulation has been carried out starting from this position (see below). We have selected 400 representative structures from four MD runs (100 structures a run) as targets for docking simulation. The results are shown in Tables S2 and S3 (ESI†) for PPAR-γ and RXR-α, respectively. Obviously, bexarotene has the same binding energy to both targets and this is in contrast with the single target case (Table 1) where bexarotene displays a higher binding affinity towards RXR-α than PPAR-γ.

Contrary to PPAR-γ and RXR-α, the binding sites of bexarotene in β-secretase are different for different docking modes. Fig. S2 (ESI†) shows the pose of bexarotene in the three lowest docking energy modes. Using these docking positions as initial configurations we have performed 3 sets of MD simulation; each set contains 10 independent MD runs (see below). Thus in total we carried out 30 MD trajectories of 200 ns. From each trajectory 50 snapshots at equilibrium were selected for the docking simulation and 1500 docking attempts have been made. Surprisingly, the binding energies to three binding sites (Fig. S2, ESI†) are the same within the error bar (Table S4, ESI†). Moreover, the binding energy of bexarotene to β-secretase does not differ from that of the PPAR-γ and RXR-α case (Tables S2–S4, ESI†). Thus, the docking to multiple targets selected from the MD simulation and from the docking to a single PDB structure (Table 2) provide almost the same binding affinity of bexarotene to PPAR-γ and β-secretase. However, for RXR-α the docking to a single PDB structure provides a higher binding affinity with ΔE_{bind} = −12.6 kcal mol^{-1}.

High binding affinity of bexarotene to PPAR-γ and RXR-α: MM-PBSA results

Binding free energy. To estimate the binding free energy ΔG_{bind} of bexarotene to PPAR-γ and RXR-α by the MM-PBSA method we have performed four independent 100 ns MD runs starting from the PDB (for PPAR-γ) and the best docking (for RXR-α) structures shown in Fig. 1. It should be noted that all MD trajectories were started from the same initial configurations but with different random seed numbers to generate different velocities fields. The all-atom root mean square displacement (RMSD) of the receptor relative to the initial structure and the interaction energy (van der Waals and electrostatic) are plotted as a function of time in Fig. 3 and Fig. S3 in ESI† for both targets.

We assumed that the system reaches equilibrium once the fluctuations of the interaction energy and RMSD have saturated around their equilibrium values. Based on this criterion, PPAR-γ and RXR-α complexed with bexarotene reached equilibrium after 10–55 ns (Fig. 3 and Fig. S3, ESI†). Snapshots collected at equilibrium, *i.e.* during the last 45–90 ns, were used for estimating the binding free energy by the MM-PBSA method. The results obtained for PPAR-γ and RXR-α depend on individual trajectories (Tables S5 and S6 in ESI†). Averaging over 4 MD runs we obtained the binding free energies ΔG_{bind} for both

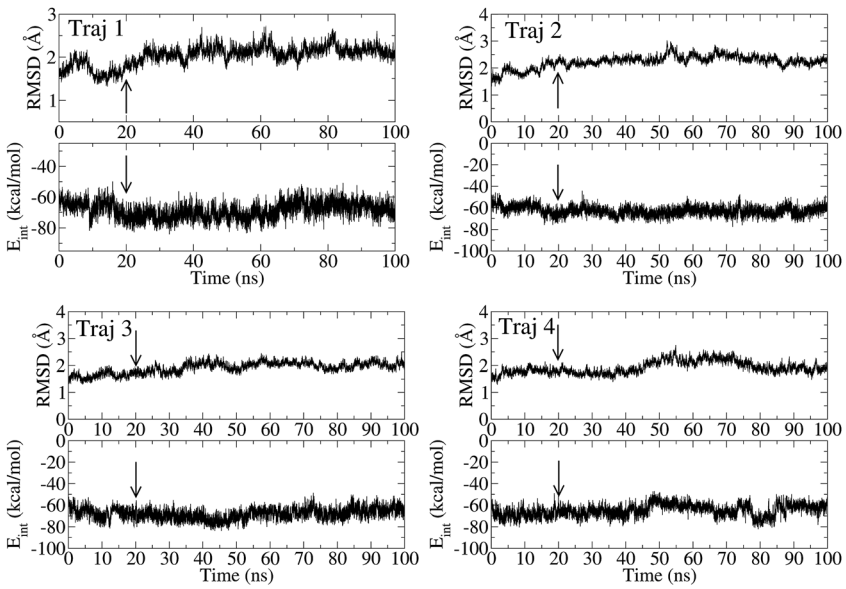

Fig. 3 Time dependence of the RMSD and the interaction energy (van der Waals and electrostatic) of the PPAR-γ + bexarotene complex. The arrow refers to the time when the system reaches equilibrium or both the RMSD and the interaction energy start to saturate.

complexes (Table 2) showing that bexarotene strongly binds not only to RXR-α but also to PPAR-γ. This result contradicts the docking simulation using a single PDB structure where bexarotene displays a poorer binding affinity to PPAR-γ compared to RXR-α (Table 2). However the MM-PBSA result agrees with the docking simulation to multiple targets obtained at equilibrium (Tables S2 and S3, ESI†) showing the same binding affinity to both targets ($\Delta E_{\mathrm{bind}} \approx -9$ kcal mol^{-1}). This agreement is due to the multiple target docking which considerably improves the crude approximations adopted in docking simulation that the receptor dynamics is ignored and the number of trials for ligand conformations is limited.

The inhibition constant IC_{50} might be roughly estimated by the formula $IC_{50} = \exp(\Delta G_{\mathrm{bind}}/RT)$, where the gas constant $R = 1.986 \times 10^{-3}$ kcal K^{-1} mol^{-1} and IC_{50} is measured in mol. Using ΔG_{bind} from Table 2 we obtain $IC_{50} \approx 0.18$ and 2.02 nM for RXR-α and PPAR-γ, respectively. Thus, bexarotene has a high binding affinity to these two targets having IC_{50} in the nanomolar range. This result is consistent with the well-known fact that bexarotene is a RXR-α agonist. Our new prediction here is that bexarotene can also tightly bind to PPAR-γ modulating its activity. The obtained data at least partially support the hypothesis presented by Cramer *et al.* that oral administration of bexarotene to the mouse model of AD resulted in Aβ clearance presumably due to enhanced expression of ApoE4.[11] ApoE has been linked to the Aβ pathology as ApoE4 binds Aβ peptides with high affinity.[48] ApoE scaffolds formation of high density lipoprotein vehicles containing cholesterol and phospholipids that promote the proteolytic clearance of Aβ peptides from the brain by microglial phagocytosis.[11] Receptors PPAR-γ, LXRs and RXRs form pairs of PPAR-γ:RXR and LXR:RXR and bind to ApoE mRNA inducing and enhancing its expression. Therefore, the strong interaction of bexarotene with PPAR-γ and RXR-α receptors may result in enhanced degradation of soluble Aβ peptides as it was shown in animal models of AD.[13]

Binding mechanism. The contributions of different terms to ΔG_{bind} are almost the same for PPAR-γ and RXR-α and for these targets the van der Waals interaction (ΔE_{vdw}) is dominating over the Coulomb interaction (ΔE_{ele}) (Table 2). In order to deeper understand the binding mechanism of bexarotene to PPAR-γ and RXR-α we have devided bexarotene into 4 groups as shown in Fig. S4 (ESI†). The interaction energy of these two proteins with different blocks of bexarotene is shown in Table S7 (ESI†). Group 2 experiences a weak repulsive electrostatic interaction with PPAR-γ, whereas such an interaction occurs between block 3 and RXR-α. Due to the large number of atoms (Fig. S4, ESI†) the contribution of group 3 to the complex stability is dominant having a total energy of about −31 kcal mol^{-1} for both targets. The most pronounced difference between the two proteins comes from the interaction with bexarotene block 2 (Table S7, ESI†) in that this block interacts with RXR-α stronger than with PPAR-γ.

The per-residue interaction energies of PPAR-γ are shown in Fig. S5 (ESI†). The strongest attractive electrostatic interaction occurs between bexarotene and residue Lys367. Eelec of residue Asp260 is lower than −2 kcal mol^{-1}, while strong repulsion is observed for residue Arg288. Residues Arg280, Ile281, Gly284, Cys285, Ile341 and Met364 dominate in the vdW interaction (Fig. S5, ESI†).

In the case of RXR-α residues Lys274, Arg316, Leu326 and Ala327 make the major contribution to the electrostatic interaction with bexarotene, while the residues Ile268, Ala271, Ala272, Leu309, Ile310, Phe313, Leu326, Ile345, Cys432 and His435 dominate in the vdW interaction (Fig. S6, ESI†).

Low binding affinity of bexarotene to β-secretase: MM-PBSA results

Binding free energy. To estimate ΔG_{bind} of bexarotene to β-secretase, we performed 3 independent MD simulation sets, starting from the three initial configurations obtained in the three best docking modes (Fig. S2, ESI†). Each set includes 10 independent MD runs. In the case of PPAR-γ and RXR-α, when bexarotene is localized in the deep binding site 100 ns was sufficient to estimate the binding free energy. However, for the β-secretase + bexarotene complex the mobility of bexarotene is higher due to the shallower binding sites (Fig. S2, ESI†) and we extended the simulation to 200 ns. Depending on MD trajectories the β-secretase + bexarotene complex reaches equilibrium at different time scales of less than 100 ns (Fig. S7–S9 in ESI†).

Using eqn (1) and snapshots collected after 100 ns we calculated ΔG_{bind} for each MD trajectory for the β-secretase target. The binding affinity depends on trajectories (Table S8 in ESI†) but overall it remains low (Table 2 and Table S8, ESI†). It should be noted that this result is inconsistent with the docking prediction (Tables S2–S4, ESI†) that bexarotene should bind to β-secretase as strongly as to PPAR-γ and RXR-α. Such a disagreement between the two methods is due to the fact that the docking simulation is much less accurate than MD. The statistical error for the MM-MBPSA binding free energy (Table 2 and Table S8, ESI†) of bexarotene to β-secretase is a factor of 2–3 larger than that of the other two proteins. This is due to the fact that bexarotene resides deeply in PPAR-γ and RXR-α leading to small fluctuations in binding free energy, whereas its weak binding to β-secretase results in large variations between different MD runs.

The poor binding propensity resulting from the MM-PBSA calculation suggests that bexarotene is not able to prevent β-secretase from its activity in cleavage of Aβ peptides from APP. In other words, bexarotene cannot reduce the Aβ production through interaction with β-secretase. As in the case of PPAR-γ and RXR-α, the vdW interaction is superior to the electrostatic interaction in directing bexarotene to bind to β-secretase.

Binding mechanism. Similar to the case of PPAR-γ and RXR-α the electrostatic interaction is less important than vdW (Table 2). The contribution of bexarotene block 3 dominates the other three blocks (Table S7, ESI†). The smallest contribution is made by the carboxyl group (block 4 in Fig. S4, ESI†) with $E_{\mathrm{elec}} + E_{\mathrm{vdW}} = -5.7$ kcal mol^{-1}.

Residue Asp32 of β-secretase makes the greatest contribution to the binding of bexarotene with $E_{\mathrm{elec}} \approx -15$ kcal mol^{-1} (Fig. 4), while residue Asp228 destabilizes the complex through

a strong repulsive electrostatic interaction with bexarotene. Residues Tyr71 and Gln73 are most prominent in the vdW interaction.

Effect of bexarotene ionization on its binding affinity to β-secretase. In previous simulations we have considered normal bexarotene with zero charge. However, since it has pK_a = 4.07 (https://www.drugbank.ca/drugs/DB00307), it is usually ionized in physiological conditions having a charge of −1, as one hydrogen atom is dissociated from the carboxyl group. The structure of ionized bexarotene is shown in Fig. S10 (ESI†). One can show that ionized bexarotene has the same position as normal bexarotene in the best three docking modes (Fig. S2, ESI†) and their binding energies are almost the same (results not shown).

We have also calculated the binding free energy of ionized bexarotene using the MM-PBSA method. For this, as in the case of normal bexarotene, three sets of ten 200 ns MD runs were performed starting from three binding poses (Fig. S2, ESI†). For mode 1 we obtained ΔG_{bind} = −3.25 ± 4.28 kcal mol^{-1} (Table S9, ESI†) and within error this value is the same as −3.57 ± 6.88 kcal mol^{-1}, obtained for normal bexarotene (Table S8, ESI†). Similar results were obtained for modes 2 and 3 (results not shown). Thus, ionization of bexarotene under physiological conditions has very little effect on its binding affinity to β-secretase. This is because the vdW interaction, but not the electrostatic interaction, is the driving force for association of bexarotene with β-secretase (Tables S8 and S9, ESI†).

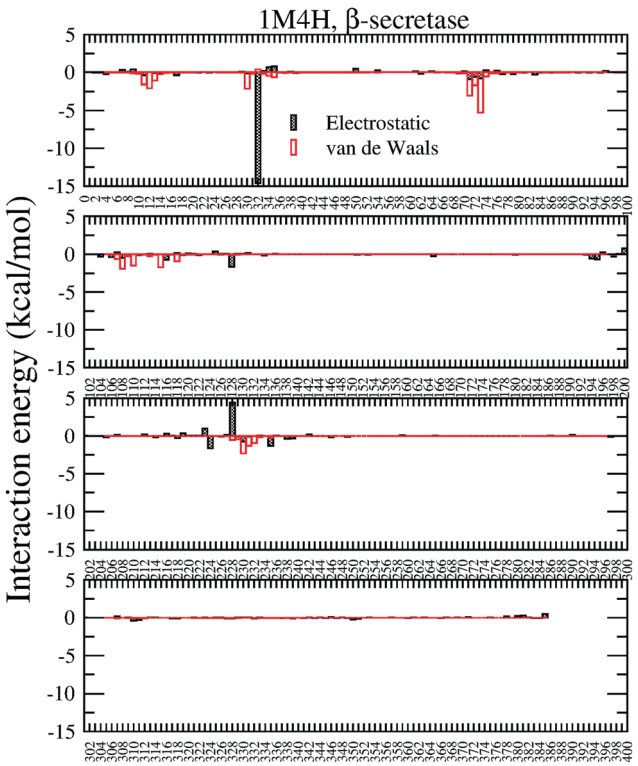

Fig. 4 Per-residue interaction energies for β-secretase. Results were averaged over 30 MD runs which were started from the three best docking modes.

Weak effect of bexarotene on β-secretase activity: *in vitro* experiment

Because results of modeling do depend on the models used, to support our *in silico* results we have tested experimentally the effect of bexarotene in the concentration range 100 pM–1 mM on inhibition of β-secretase activity using a β-secretase (BACE-1) Fret Assay Kit. The standard assay protocol was designed to convert approximately 10% of substrate (Rh-EVNLDAEFK-Quencher) to product. As a positive control peptide product (Rh-EVNL) was used to represent 100% conversion. Substrate was added to the product to account for any fluorescence that was absorbed by the quencher groups (negative control). These controls indicate that observed fluorescence intensities are a result of the bexarotene effect on β-secretase. Our results suggest that bexarotene has no inhibitory effect on β-secretase activity as the obtained fluorescence intensities (Fig. 5) for the whole bexarotene concentration range are similar to the fluorescence intensities of BACE-1 product (rhodamine-EVNL; taken as 100%). These *in vitro* data are thus consistent with *in silico* predictions on poor binding toward β-secretase.

A number of studies have indicated that changes in the level and activity of β-secretase induce or inhibit generation of toxic Aβ peptides. Luo *et al.* have suggested that BACE1 deficiency in AD model mice reduces levels of Aβ peptides, rescues neuronal loss and improves memory deficits.[49] Importantly, its inhibition by small molecules would halt the formation of Aβ at the very beginning, thus slowing significantly progression of AD. Eketjall *et al.* have reported recently that AZD3293, a highly permeable, orally active, blood–brain barrier penetrating, BACE1 inhibitor with unique slow off-rate kinetics displayed significant dose- and time-dependent reductions in plasma, cerebrospinal fluid, and brain concentrations of $A\beta_{40}$, $A\beta_{42}$, and sAβPPβ *in vivo* in mice, guinea pigs, and dogs.[50] However, weak interaction with β-secretase implies that bexarotene cannot influence its level or activity and thus cannot prevent the production of Aβ peptides. Therefore the reduction of neurotoxic plaques due to this mechanism is very unlikely.

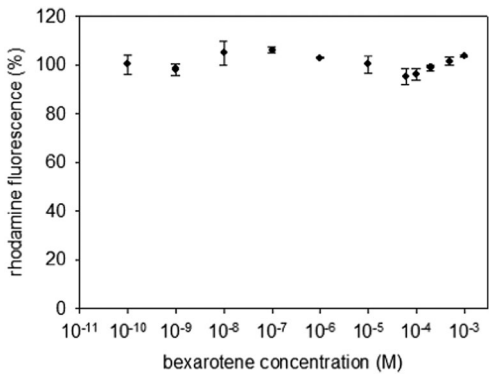

Fig. 5 Effect of bexarotene on β-secretase activity determined as the fluorescence of rhodamine using a (BACE-1) FRET Assay Kit. The error bars represent the standard deviation from the average values of three independent samples.

Conclusion

Bexarotene may play an important role in treatment of AD, but its activity is not completely understood. We have performed a comprehensive analysis of its binding affinity to three targets, which can affect Aβ clearance, namely to peroxisome proliferator-activated receptor γ (PPAR-γ), retinoid X receptors (RXRs) and β-secretase. The results obtained by *in silico* and *in vitro* experiments show that bexarotene weakly binds to β-secretase indicating that bexarotene-induced clearance of amyloid plaques is probably not through inhibition of Aβ production. Our simulation indicated that ionization of bexarotene under physiological conditions does not change its binding affinity to β-secretase. We have also shown that bexarotene can tightly bind not only to RXR-α but also to PPAR-γ with the inhibition constant in the sub-nanomolar range. This result is consistent with the pathway of efficient Aβ clearance through ApoE4 overexpression due to activation of PPAR-γ or both receptors. There exist several inhibitors of γ-secretase[51] which is responsible for the final step in Aβ generation. However, a possibility of preventing Aβ production by bexarotene-induced inhibition of γ-secretase activity has not been explored. Our work on this problem is in progress.

Conflicts of interest

There are no conflicts to declare.

Acknowledgements

The work was supported by Narodowe Centrum Nauki in Poland (Grant No. 2015/19/B/ST4/02721) and Department of Science and Technology at Ho Chi Minh City, Vietnam. Allocation of CPU time at the supercomputer center TASK in Gdansk (Poland) is highly appreciated. We acknowledge PRACE for awarding us access, within the DECI 13th call, to the Eagle HPC cluster based in Poland at Poznan. In Slovakia the work was supported by research grants SAS-MOST JRP2015/5, VEGA 2/0145/17, 2/0030/18 and MVTS NGP-NET - BM1405.

References

1 J. A. Hardy and G. A. Higgins, Alzheimers-disease - the amyloid cascade hypothesis, *Science*, 1992, **256**, 184–185.
2 J. Nasica-Labouze, P. H. Nguyen, F. Sterpone, O. Berthoumieu, N. V. Buchete, S. Cote, A. De Simone, A. J. Doig, P. Faller, A. Garcia, A. Laio, M. S. Li, S. Melchionna, N. Mousseau, Y. G. Mu, A. Paravastu, S. Pasquali, D. J. Rosenman, B. Strodel, B. Tarus, J. H. Viles, T. Zhang, C. Y. Wang and P. Derreumaux, Amyloid beta Protein and Alzheimer's Disease: When Computer Simulations Complement Experimental Studies, *Chem. Rev.*, 2015, **115**, 3518–3563.
3 R. J. O'Brien and P. C. Wong, Amyloid precursor protein processing and Alzheimer's disease, *Annu. Rev. Neurosci.*, 2011, **34**, 185–204.
4 M. P. Mattson, Cellular actions of beta-amyloid precursor protein and its soluble and fibrillogenic derivatives, *Physiol. Rev.*, 1997, **77**, 1081–1132.
5 M. Ohno, S. L. Cole, M. Yasvoina, J. Zhao, M. Citron, R. Berry, J. F. Disterhoft and R. Vassar, BACE1 gene deletion prevents neuron loss and memory deficits in 5XFAD APP/PS1 transgenic mice, *Neurobiol. Dis.*, 2007, **26**, 134–145.
6 L.-B. Yang, K. Lindholm, R. Yan, M. Citron, W. Xia, X.-L. Yang, T. Beach, L. Sue, P. Wong and D. Price, Elevated β-secretase expression and enzymatic activity detected in sporadic Alzheimer disease, *Nat. Med.*, 2003, **9**, 3–4.
7 D. Dominguez, J. Tournoy, D. Hartmann, T. Huth, K. Cryns, S. Deforce, L. Serneels, I. E. Camacho, E. Marjaux and K. Craessaerts, Phenotypic and biochemical analyses of BACE1-and BACE2-deficient mice, *J. Biol. Chem.*, 2005, **280**, 30797–30806.
8 Y.-w. Zhang, R. Thompson, H. Zhang and H. Xu, APP processing in Alzheimer's disease, *Mol. Brain*, 2011, **4**, 3.
9 K. Ghosal, M. Haag, P. B. Verghese, T. West, T. Veenstra, J. B. Braunstein, R. J. Bateman, D. M. Holtzman and G. E. Landreth, A randomized controlled study to evaluate the effect of bexarotene on amyloid-β and apolipoprotein E metabolism in healthy subjects, *Alzheimer's Dementia*, 2016, **2**, 110–120.
10 R. Gniadecki, C. Assaf, M. Bagot, R. Dummer, M. Duvic, R. Knobler, A. Ranki, P. Schwandt and S. Whittaker, The optimal use of bexarotene in cutaneous T-cell lymphoma, *Br. J. Dermatol.*, 2007, **157**, 433–440.
11 P. E. Cramer, J. R. Cirrito, D. W. Wesson, C. D. Lee, J. C. Karlo, A. E. Zinn, B. T. Casali, J. L. Restivo, W. D. Goebel and M. J. James, ApoE-directed therapeutics rapidly clear β-amyloid and reverse deficits in AD mouse models, *Science*, 2012, **335**, 1503–1506.
12 F. M. LaFerla, Preclinical success against Alzheimer's disease with an old drug, *N. Engl. J. Med.*, 2012, **367**, 570–572.
13 N. Fitz, A. Cronican, I. Lefterov and R. Koldamova, Comment on ''ApoE-directed therapeutics rapidly clear β-amyloid and reverse deficits in AD mouse models'', *Science*, 2013, **340**, 924-c.
14 A. R. Price, G. Xu, Z. B. Siemienski, L. A. Smithson, D. R. Borchelt, T. E. Golde and K. M. Felsenstein, Comment on ''ApoE-Directed Therapeutics Rapidly Clear beta-Amyloid and Reverse Deficits in AD Mouse Models'', *Science*, 2013, **340**, 924.
15 I. Tesseur, A. Lo, A. Roberfroid, S. Dietvorst, B. Van Broeck, M. Borgers, H. Gijsen, D. Moechars, M. Mercken and J. Kemp, Comment on ''ApoE-directed therapeutics rapidly clear β-amyloid and reverse deficits in AD mouse models'', *Science*, 2013, **340**, 924-e.
16 K. Veeraraghavalu, C. Zhang, S. Miller, J. K. Hefendehl, T. W. Rajapaksha, J. Ulrich, M. Jucker, D. M. Holtzman, R. E. Tanzi and R. Vassar, Comment on ''ApoE-directed therapeutics rapidly clear β-amyloid and reverse deficits in AD mouse models'', *Science*, 2013, **340**, 924.
17 A. S. Dickey, D. N. Sanchez, M. Arreola, K. R. Sampat, W. Fan, N. Arbez, S. Akimov, M. J. Van Kanegan, K. Ohnishi, S. K. Gilmore-Hall, A. L. Flores, J. M. Nguyen, N. Lomas,

C. L. Hsu, D. C. Lo, C. A. Ross, E. Masliah, R. M. Evans and A. R. La Spada, PPARδ activation by bexarotene promotes neuroprotection by restoring bioenergetic and quality control homeostasis, *Sci. Transl. Med.*, 2017, **9**, eaal2332.

18 J. Fantini, C. Di Scala, N. Yahi, J. D. Troadec, K. Sadelli, H. Chahinian and N. Garmy, Bexarotene Blocks Calcium-Permeable Ion Channels Formed by Neurotoxic Alzheimer's beta-Amyloid Peptides, *ACS Chem. Neurosci.*, 2014, **5**, 216–224.

19 S. Wajid, S. Khowal and S. Chandra, In-silico scrutiny and molecular docking analysis for beta secretase-1 and presenilin-1, *J. Pharm. BioSci.*, 2014, **5**, 274–292.

20 P. D. Q. Huy, N. Q. Thai, Z. Bednarikova, L. H. Phuc, H. Q. Linh, Z. Gazova and M. S. Li, Bexarotene does not clear amyloid beta plaques but delays fibril growth: Molecular mechanisms, *ACS Chem. Neurosci.*, 2017, **8**, 1960–1969.

21 J. Habchi, P. Arosio, M. Perni, A. R. Costa, M. Yagi-Utsumi, P. Joshi, S. Chia, S. I. A. Cohen, M. B. D. Muller, S. Linse, E. A. A. Nollen, C. M. Dobson, T. P. J. Knowles and M. Vendruscolo, An anticancer drug suppresses the primary nucleation reaction that initiates the production of the toxic Abeta 42 aggregates linked with Alzheimer's disease, *Sci. Adv.*, 2016, **2**, e1501244.

22 J. Habchi, S. Chia, R. Limbocker, B. Mannini, M. Ahn, M. Perni, O. Hansson, P. Arosio, J. R. Kumita, P. K. Challa, S. I. A. Cohen, S. Linse, C. M. Dobson, T. P. J. Knowles and M. Vendruscolo, Systematic development of small molecules to inhibit specific microscopic steps of A beta 42 aggregation in Alzheimer's disease, *Proc. Natl. Acad. Sci. U. S. A.*, 2017, **114**, E200–E208.

23 P. A. Kollman, I. Massova, C. Reyes, B. Kuhn, S. Huo, L. Chong, M. Lee, T. Lee, Y. Duan and W. Wang, Calculating structures and free energies of complex molecules: combining molecular mechanics and continuum models, *Acc. Chem. Res.*, 2000, **33**, 889–897.

24 M. Frisch, G. Trucks, H. Schlegel, G. Scuseria, M. Robb, J. Cheeseman, G. Scalmani, V. Barone, B. Mennucci and G. Petersson: *Gaussian 09, revision D. 01*, Gaussian, Inc., Wallingford CT, 2009.

25 C. C. J. Roothaan, New development of molecular orbital theory, *Rev. Mod. Phys.*, 1951, **23**, 69–89.

26 U. C. Singh and P. A. Kollman, An approach to computing electrostatic charges for molecules, *J. Comput. Chem.*, 1984, **5**, 129–145.

27 B. H. Besler, K. M. Merz and P. A. Kollman, Atomic charges derived from semiempirical methods, *J. Comput. Chem.*, 1990, **11**, 431–439.

28 M. V. Liberato, A. S. Nascimento, S. D. Ayers, J. Z. Lin, A. Cvoro, R. L. Silveira, L. Martínez, P. C. Souza, D. Saidemberg and T. Deng, Medium chain fatty acids are selective peroxisome proliferator activated receptor (PPAR) γ activators and pan-PPAR partial agonists, *PLoS One*, 2012, **7**, e36297.

29 L. J. Boerma, G. Xia, C. Qui, B. D. Cox, M. J. Chalmers, C. D. Smith, S. Lobo-Ruppert, P. R. Griffin, D. D. Muccio and M. B. Renfrow, Defining the communication between agonist and coactivator binding in the retinoid X receptor α ligand binding domain, *J. Biol. Chem.*, 2014, **289**, 814–826.

30 L. Hong, R. T. Turner, G. Koelsch, D. Shin, A. K. Ghosh and J. Tang, Crystal structure of memapsin 2 (β-secretase) in complex with an inhibitor OM00-3, *Biochemistry*, 2002, **41**, 10963–10967.

31 M. F. Sanner, Python: a programming language for software integration and development, *J. Mol. Graphics Modell.*, 1999, **17**, 57–61.

32 A. Vina, Improving the speed and accuracy of docking with a new scoring function, efficient optimization, and multithreading Trott, Oleg; Olson, Arthur, *J. Comput. Chem.*, 2010, **31**, 455–461.

33 V. Hornak, R. Abel, A. Okur, B. Strockbine, A. Roitberg and C. Simmerling, Comparison of multiple Amber force fields and development of improved protein backbone parameters, *Proteins: Struct., Funct., Bioinf.*, 2006, **65**, 712–725.

34 D. A. Case, T. E. Cheatham, T. Darden, H. Gohlke, R. Luo, K. M. Merz, A. Onufriev, C. Simmerling, B. Wang and R. J. Woods, The Amber biomolecular simulation programs, *J. Comput. Chem.*, 2005, **26**, 1668–1688.

35 W. L. Jorgensen, J. Chandrasekhar, J. D. Madura, R. W. Impey and M. L. Klein, Comparison of simple potential functions for simulating liquid water, *J. Chem. Phys.*, 1983, **79**, 926–935.

36 W. F. van Gunsteren; S. R. Billeter; A. A. Eising; P. H. Hünenberger; P. Krüger; A. E. Mark; W. R. Scott and I. G. Tironi, Biomolecular simulation: the {GROMOS96} manual and user guide, 1996.

37 T. T. Nguyen, M. H. Viet and M. S. Li, Effects of water models on binding affinity: evidence from all-atom simulation of binding of tamiflu to A/H5N1 neuraminidase, *Sci. World J.*, 2014, 536084.

38 R. Hockney, S. Goel and J. Eastwood, Quiet high-resolution computer models of a plasma, *J. Comput. Phys.*, 1974, **14**, 148–158.

39 J.-P. Ryckaert, G. Ciccotti and H. J. Berendsen, Numerical integration of the cartesian equations of motion of a system with constraints: molecular dynamics of *n*-alkanes, *J. Comput. Phys.*, 1977, **23**, 327–341.

40 X. Wu and B. R. Brooks, Self-guided Langevin dynamics simulation method, *Chem. Phys. Lett.*, 2003, **381**, 512–518.

41 T. Darden, D. York and L. Pedersen, Particle mesh Ewald: An N log (N) method for Ewald sums in large systems, *J. Chem. Phys.*, 1993, **98**, 10089–10092.

42 S. T. Ngo and M. S. Li, Curcumin binds to Aβ1–40 peptides and fibrils stronger than ibuprofen and naproxen, *J. Phys. Chem. B*, 2012, **116**, 10165–10175.

43 M. H. Viet, S. T. Ngo, N. S. Lam and M. S. Li, Inhibition of aggregation of amyloid peptides by beta-sheet breaker peptides and their binding affinity, *J. Phys. Chem. B*, 2011, **115**, 7433–7446.

44 T. T. Nguyen, B. K. Mai and M. S. Li, Study of Tamiflu sensitivity to variants of A/H5N1 virus using different force fields, *J. Chem. Inf. Model.*, 2011, **51**, 2266–2276.

45 D. A. McQuarrie, *Statistical thermodynamics*, 1973.

46 R. A. Laskowski and M. B. Swindells, *LigPlot +: multiple ligand–protein interaction diagrams for drug discovery*. ACS Publications, 2011.
47 P. Chambon, A decade of molecular biology of retinoic acid receptors, *FASEB J.*, 1996, **10**, 940–954.
48 W. J. Strittmatter, K. H. Weisgraber, D. Y. Huang, L.-M. Dong, G. S. Salvesen, M. Pericak-Vance, D. Schmechel, A. M. Saunders, D. Goldgaber and A. D. Roses, Binding of human apolipoprotein E to synthetic amyloid beta peptide: isoform-specific effects and implications for late-onset Alzheimer disease, *Proc. Natl. Acad. Sci. U. S. A.*, 1993, **90**, 8098–8102.
49 Y. Luo, B. Bolon, S. Kahn, B. D. Bennett, S. Babu-Khan, P. Denis, W. Fan, H. Kha, J. Zhang and Y. Gong, Mice deficient in BACE1, the Alzheimer's [beta]-secretase, have normal phenotype and abolished [beta]-amyloid generation, *Nat. Neurosci.*, 2001, **4**, 231.
50 S. Eketjäll, J. Janson, K. Kaspersson, A. Bogstedt, F. Jeppsson, J. Fälting, S. B. Haeberlein, A. R. Kugler, R. C. Alexander and G. Cebers, AZD3293: A novel, orally active BACE1 inhibitor with high potency and permeability and markedly slow off-rate kinetics, *J. Alzheimer's Dis.*, 2016, **50**, 1109–1123.
51 F. Mangialasche, A. Solomon, B. Winblad, P. Mecocci and M. Kivipelto, Alzheimer's disease: clinical trials and drug development, *Lancet Neurol.*, 2010, **9**, 702–716.

Supporting information for: Bexarotene cannot reduce amyloid beta plaques through inhibition of production of amyloid beta peptides: *In silico* and *in vitro* study

Pham Dinh Quoc Huy,[1,2] Nguyen Quoc Thai,[2,3,4] Zuzana Bednarikova,[5] Huynh Quang Linh,[4] Zuzana Gazova,[5] and Mai Suan Li[1]

[1]Institute of Physics, Polish Academy of Sciences, Al. Lotnikow 32/46, 02-668, Warsaw, Poland,
[2]Institute for Computational Science and Technology, Quang Trung Software City, Tan Chanh Hiep Ward, District 12, Ho Chi Minh City, Vietnam,
[3]Division of Theoretical Physics, Dong Thap University, 783 Pham Huu Lau Str., Ward 6, Cao Lanh City, Dong Thap, Vietnam,
[4]Biomedical Engineering Department, University of Technology - VNU HCM 268 Ly Thuong Kiet Str., Distr. 10, Ho Chi Minh City, Vietnam,
[5]Department of Biophysics, Institute of Experimental Physics, Slovak Academy of Sciences, Watsonova 47, 040 01 Kosice, Slovakia

E-mail: masli@ifpan.edu.pl; gazova@saske.sk

Table S1: Atom name, atom type, and charge of bexarotene.

Num.	Atom name	Atom Type	Charge
1	C1	CT	-0.077810
2	C2	CT	0.537189
3	C3	CT	-0.110215
4	C4	CA	-0.071271
5	C5	CA	-0.140981
6	C6	CA	-0.384321
7	C7	CT	0.561644
8	C8	CA	-0.246028
9	C9	CA	0.215507
10	C10	CA	0.072981
11	H1	HC	0.005864
12	H2	HC	0.005864
13	H3	HC	0.014390
14	H4	HC	0.014390
15	H5	HA	0.193910
16	H6	HA	0.149062
17	C11	CD	-0.053301
18	C12	CM	-0.390605
19	H7	HA	0.165233
20	H8	HA	0.165233
21	C13	CA	0.204433
22	C14	CA	-0.189451
23	C15	CA	-0.130122
24	H9	HA	0.144582
25	C16	CA	-0.165782
26	H10	HA	0.149271
27	C17	CA	-0.130122
28	C18	CA	-0.189451
29	H11	HA	0.149271
30	H12	HA	0.144582
31	C19	C	0.820182
32	O1	O	-0.541187
33	O2	OH	-0.635151
34	H13	HO	0.407750
35	C20	CT	-0.322763
36	H14	HC	0.092808
37	H15	HC	0.092808
38	H16	HC	0.092808
39	C21	CT	-0.423075
40	H17	HC	0.089443
41	H18	HC	0.089443
42	H19	HC	0.089443
43	C22	CT	-0.423075
44	H20	HC	0.089443
45	H21	HC	0.089443
46	H22	HC	0.089443
47	C23	CT	-0.430289
48	H23	HC	0.091479
49	H24	HC	0.091479
50	H25	HC	0.091479
51	C24	CT	-0.430289
52	H26	HC	0.091479
53	H27	HC	0.091479
54	H28	HC	0.091479

Table S2: Results for docking of bexarotene to equilibrium structures of receptor PPAR-γ. In each MD trajectory, a set of 100 structures of PPAR-γ, collected regularly at equilibration, were used to dock with bexarotene. Totally 400 docking attempts were made.

PPAR-γ	
Trajectory	Average of binding affinity over snapshots in each trajectory (kcal/mol)
Traj 1	-9.09 +/- 0.81
Traj 2	-8.71 +/- 0.80
Traj 3	-9.17 +/- 0.79
Traj 4	-8.75 +/- 1.02
Average over all trajectories	**-8.93 +/- 0.23**

Table S3: The same as table S2 but for receptor RXR-α. Totally 400 docking attempts were made.

RXR-alpha	
Trajectory	Average of binding affinity over snapshots in each trajectory (kcal/mol)
Traj 1	-9.07 +/- 1.60
Traj 2	-8.29 +/- 1.54
Traj 3	-8.99 +/- 1.70
Traj 4	-9.39 +/- 1.64
Average over all trajectories	**-8.94 +/- 0.46**

Table S4 : Docking energy of bexarotene to β-secreatse. Results were obtained from 1500 docking attempts using snapshots collected at equibrium in 30 MD runs as targets (see the main text for more details).

Beta-secretase docking		
Mode	Trajectory	Average binding affinity (kcal/mol)
Mode 1	Traj 1	-7.72 +/- 0.45
	Traj 2	-8.11 +/- 0.63
	Traj 3	-9.00 +/- 0.81
	Traj 4	-8.82 +/- 0.45
	Traj 5	-8.78 +/- 0.95
	Traj 6	-8.80 +/- 0.75
	Traj 7	-8.38 +/- 0.65
	Traj 8	-9.12 +/- 0.81
	Traj 9	-7.78 +/- 0.48
	Traj 10	-7.94 +/- 0.46
	Average over mode 1	**-8.45 +/- 0.53**
Mode 2	Traj 1	-7.86+/- 0.56
	Traj 2	-7.70 +/- 0.41
	Traj 3	-7.48 +/- 0.38
	Traj 4	-7.89 +/- 0.58
	Traj 5	-7.63 +/- 0.39
	Traj 6	-8.72 +/- 0.78
	Traj 7	-7.71 +/- 0.58
	Traj 8	-8.10 +/- 0.64
	Traj 9	-7.77 +/- 0.49
	Traj 10	-7.77 +/- 0.59
	Average over mode 1	**-7.86 +/- 0.34**
Mode 3	Traj 1	-7.87 +/- 0.50
	Traj 2	-7.72 +/- 0.40
	Traj 3	-7.85 +/- 0.56
	Traj 4	-7.75 +/- 0.40
	Traj 5	-7.76 +/- 0.49
	Traj 6	-7.73 +/- 0.50
	Traj 7	-8.00 +/- 0.51
	Traj 8	-7.89 +/- 0.44
	Traj 9	-7.54 +/- 0.43
	Traj 10	-7.77 +/- 0.40
	Average over mode 3	**-7.79 +/- 0.12**
Average over all modes		**-8.03 +/- 0.46**

Table S5: Binding free energy of bexarotene to PPAR-γ. See Fig. 3 in the main text for evolution of RMSD and interaction energy.

Traj	ΔE_{vdW}	ΔE_{ele}	ΔG_{PB}	ΔG_{SUR}	$-T\Delta S$	ΔG_{bind}
1	-50.0	-19.3	35.5	-4.5	19.6	-18.7
2	-48.6	-14.9	30.3	-4.5	22.4	-15.3
3	-50.7	-17.6	36.0	-4.5	20.9	-15.9
4	-49.8	-14.4	36.5	-4.7	17.6	-14.8
Average	-49.8±0.9	-16.5±2.3	34.6±2.9	-4.6±0.1	20.1±1.4	-16.2±1.8

Table S6: Binding free energy of bexarotene to RXR-α. See Fig. S1 in SI for the evolution of RMSD and interaction energy.

Traj	ΔE_{vdW}	ΔE_{ele}	ΔG_{PB}	ΔG_{SUR}	$-T\Delta S$	ΔG_{bind}
1	-52.6	-17.5	38.9	-4.5	20.9	-14.9
2	-55.8	-14.9	34.0	-4.4	20.4	-20.6
3	-53.0	-17.8	39.2	-4.5	17.9	-18.1
4	-52.9	-20.4	42.7	-4.5	21.0	-14.1
Average	-53.6±1.5	-17.6±2.3	38.7±3.6	-4.5±0.1	20.1±1.4	-16.9±3.0

Table S7. Decomposition of the interaction energy into 4 groups of bexarotene (Figure S4). For PPAR-γ (4EMA) and RXR-α (4K6I) the results were averaged over four MD trajectories, while for β-secreatase (1M4H) the average over 30 trajectories of 3 modes was made.

		E_{elec}	E_{vdW}	$E_{elec} + E_{vdW}$
4EMA	Group 1	-10.49	-6.22	-16.70
	Group 2	0.77	-10.79	-10.02
	Group 3	-1.86	-29.50	-31.36
	Group 4	-4.95	-3.28	-8.24
4K6I	Group 1	-10.01	-6.24	-16.25
	Group 2	-2.87	-12.54	-15.41
	Group 3	0.17	-30.94	-30.77
	Group 4	-4.94	-3.84	-8.78
1M4H	Group 1	-3.26	-2.46	-5.72
	Group 2	-2.03	-6.34	-8.38
	Group 3	0.21	-15.29	-15.08
	Group 4	-5.07	-2.39	-7.45

Table S8: Binding free energy ,by MMPBSA method, between beta-secretase and bexarotene. Snapshots from the last 100ns were used to estimate the binding free energy (kcal/mol).

		ΔE_{vdW}	ΔE_{ele}	ΔG_{SUR}	ΔG_{PB}	$-T\Delta S$	ΔG_{bind}	Average
Mode 1	Traj 1	-31.40	-13.05	-3.89	33.08	12.57	-2.70	**-3.57 ± 6.88**
	Traj 2	-36.69	-12.14	-4.17	39.38	13.89	0.28	
	Traj 3	-39.79	-21.65	-4.50	45.40	16.56	-3.98	
	Traj 4	-31.44	-26.58	-4.01	42.17	16.43	-3.43	
	Traj 5	-40.51	-20.88	-4.53	45.06	7.37	-13.50	
	Traj 6	-39.38	-19.69	-4.31	40.32	22.14	-0.92	
	Traj 7	-37.05	-5.60	-4.00	27.76	9.11	-9.78	
	Traj 8	-37.73	-27.11	-4.32	46.07	10.09	-13.00	
	Traj 9	-28.99	-12.38	-3.69	30.70	18.06	3.70	
	Traj 10	-27.86	-1.57	-3.59	23.36	17.24	7.59	
Mode 2	Traj 1	-20.43	-6.09	-2.31	18.11	16.48	5.77	**-0.46 ± 7.24**
	Traj 2	-21.63	-9.65	-2.44	19.95	21.74	7.97	
	Traj 3	-25.35	-7.95	-2.90	18.98	18.35	1.13	
	Traj 4	-29.00	-2.48	-3.10	17.00	19.36	1.78	
	Traj 5	-16.13	-3.07	-1.92	10.54	16.03	5.45	
	Traj 6	-44.93	-6.50	-4.47	22.89	15.75	-17.26	
	Traj 7	-25.58	-10.17	-2.98	21.54	12.75	-4.44	
	Traj 8	-25.59	-12.92	-2.88	22.72	17.98	-0.69	
	Traj 9	-18.81	-5.25	-2.26	15.66	11.33	0.66	
	Traj 10	-22.93	-16.37	-2.81	25.34	11.84	-4.93	
Mode 3	Traj 1	-19.83	-6.73	-2.30	17.62	15.79	4.54	**2.34 ± 2.12**
	Traj 2	-19.32	-9.06	-2.38	19.26	12.89	1.39	
	Traj 3	-19.93	-1.03	-2.53	9.63	16.62	2.76	
	Traj 4	-12.31	-3.84	-1.60	9.57	10.19	2.00	
	Traj 5	-14.78	-5.82	-1.88	12.87	7.98	-1.63	
	Traj 6	-21.79	-9.38	-2.62	20.23	17.59	4.02	
	Traj 7	-25.33	-5.89	-2.88	20.84	17.39	4.14	
	Traj 8	-20.88	-9.70	-2.48	19.45	14.03	0.41	
	Traj 9	-13.30	-7.34	-1.49	14.76	12.30	4.93	
	Traj 10	-25.84	-9.63	-2.94	20.89	18.35	0.84	
Average		-26.48 ± 8.78	-10.32 ± 6.95	-3.07 ± 0.92	24.37 ± 10.97	14.94 ± 3.82	**-0.56 ± 6.20**	

Table S9: Binding free energy ,by MMPBSA method, between beta-secretase and ionized bexarotene. Snapshots from the last 100ns were used to estimate the binding free energy (kcal/mol). Results were obtained for mode 1.

Traj.	ΔE_{vdw}	ΔE_{ele}	ΔG_{PB}	ΔG_{SUR}	$-T\Delta S$	ΔG_{bind}
1	-33.76	105.44	-83.97	-3.93	12.18	-4.04
2	-34.69	98.87	-76.67	-3.90	9.50	-6.88
3	-33.99	37.73	-18.46	-4.42	15.10	-4.05
4	-34.94	119.94	-96.93	-3.93	11.77	-4.10
5	-36.20	132.87	-110.10	-3.95	13.56	-3.82
6	-35.57	118.60	-95.81	-3.96	21.65	+4.91
7	-31.39	90.19	-72.29	-3.78	21.15	+3.87
8	-35.33	103.51	-75.52	-4.10	6.93	-4.50
9	-31.79	82.45	-65.77	-3.89	10.77	-8.23
10	-38.18	98.21	-71.05	-4.05	9.41	-5.66
average	-34.58±2.01	98.78±26.11	-76.66±24.74	-3.99±0.18	13.20±4.88	**-3.25±4.28**

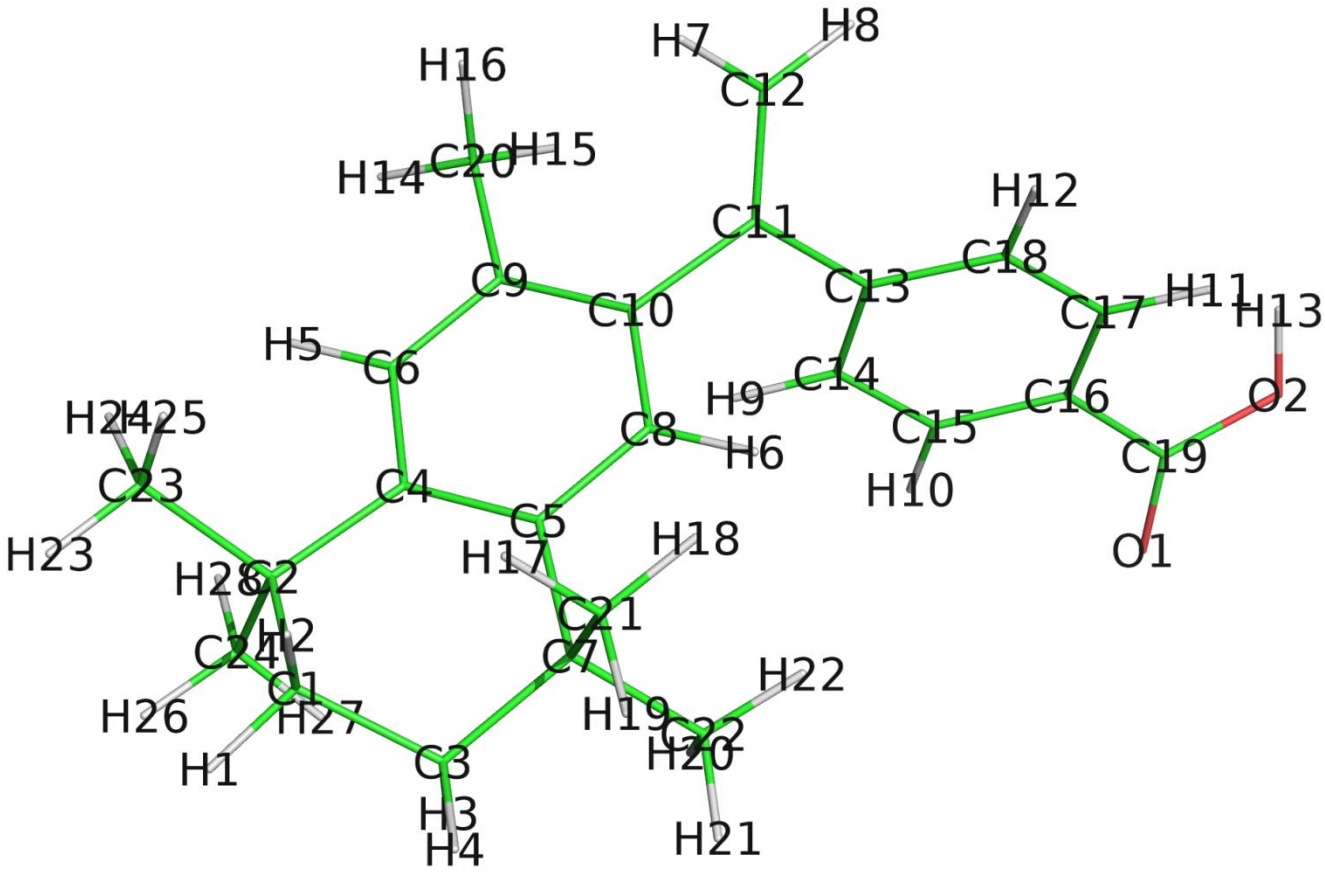

Figure S1: Structure of bexarotene which was optimized by Gaussian version 09 with the use of Hatree-Fock method and basis set 6-31G*.

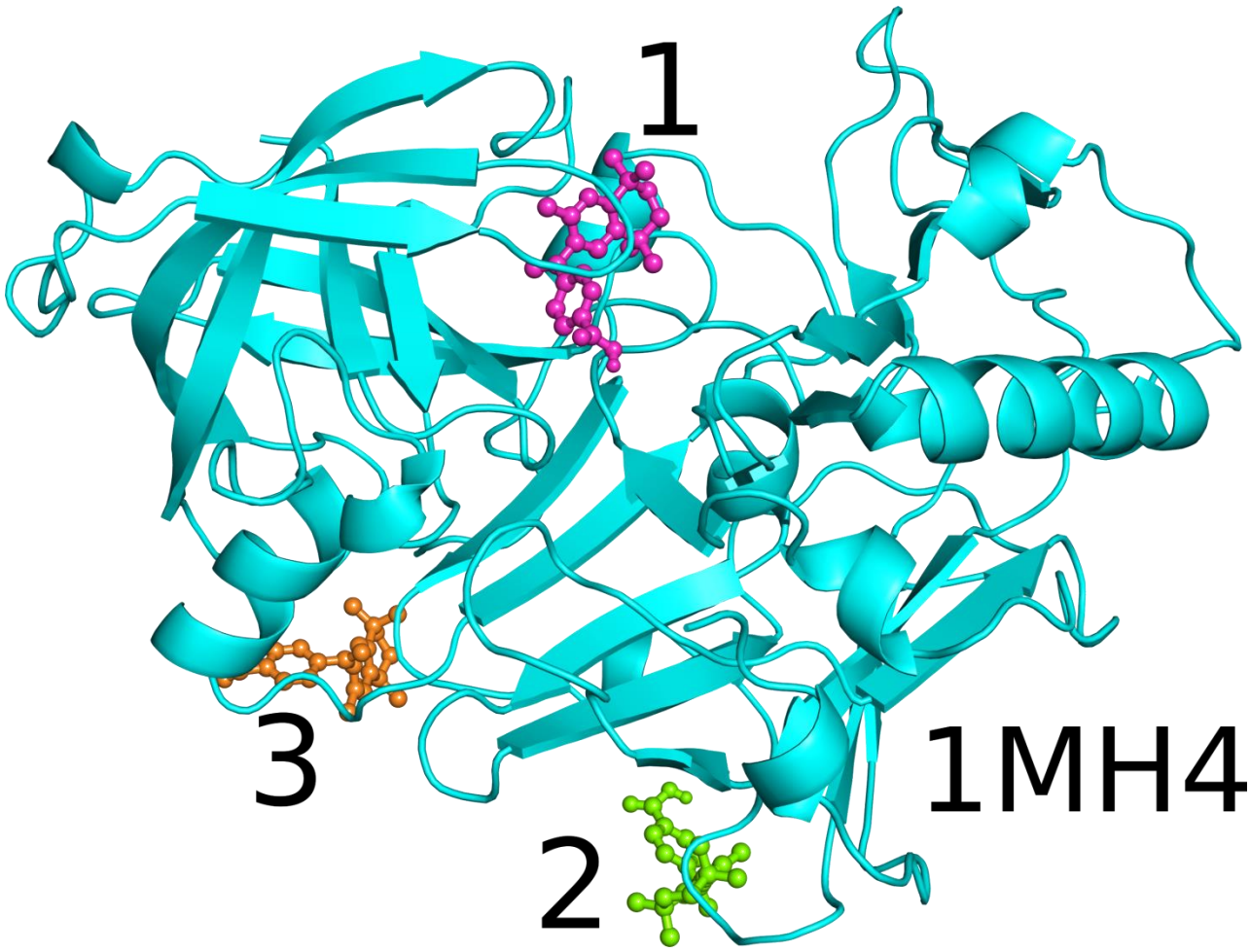

Figure S2. Three best docking modes (1, 2 and 3) of bexarotene to β-secretase. These binding positions have been used as starting configurations for three independent sets of MD simulation.

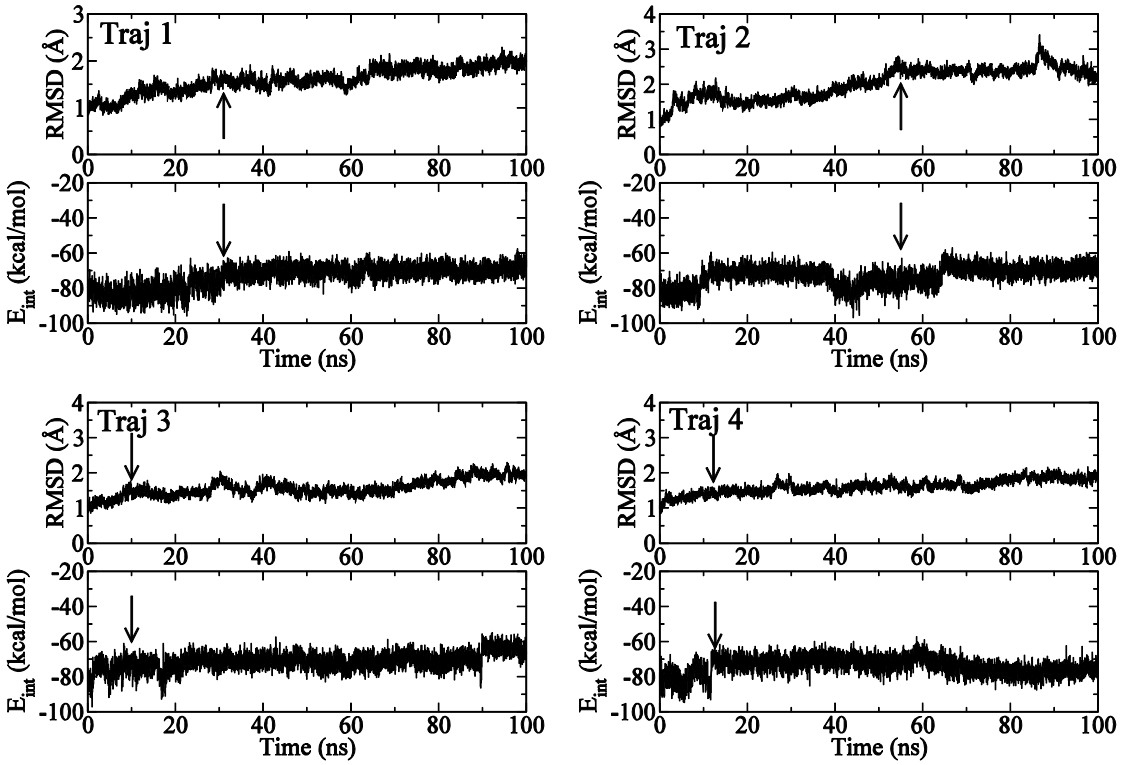

Figure S3: Time dependence of RMSD and the interaction energy of RXR-α+bexarotene complex. The arrow indicates time when the complex reaches equilibrium

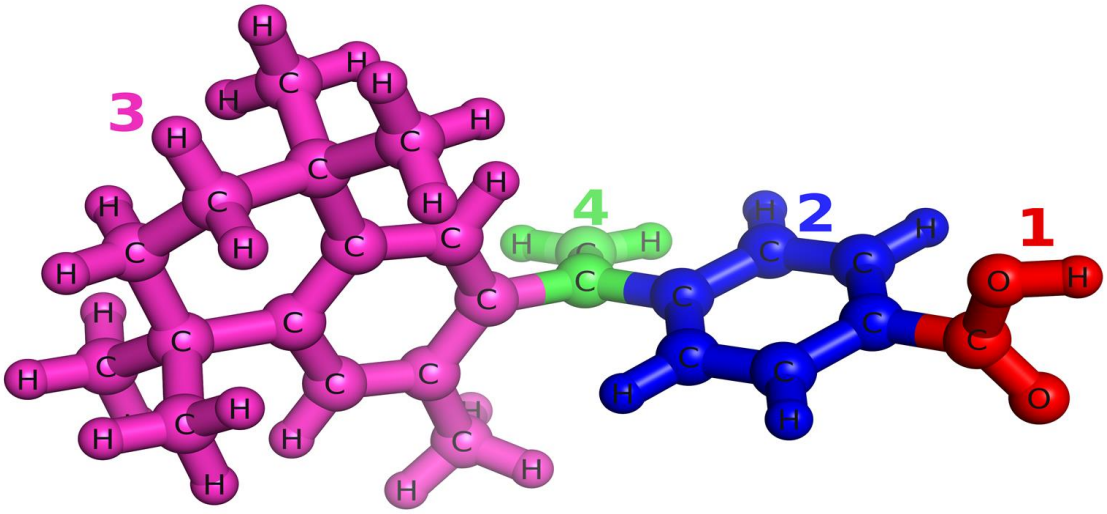

Figure S4. Bexarotene is divided into four groups denoted by different colors.

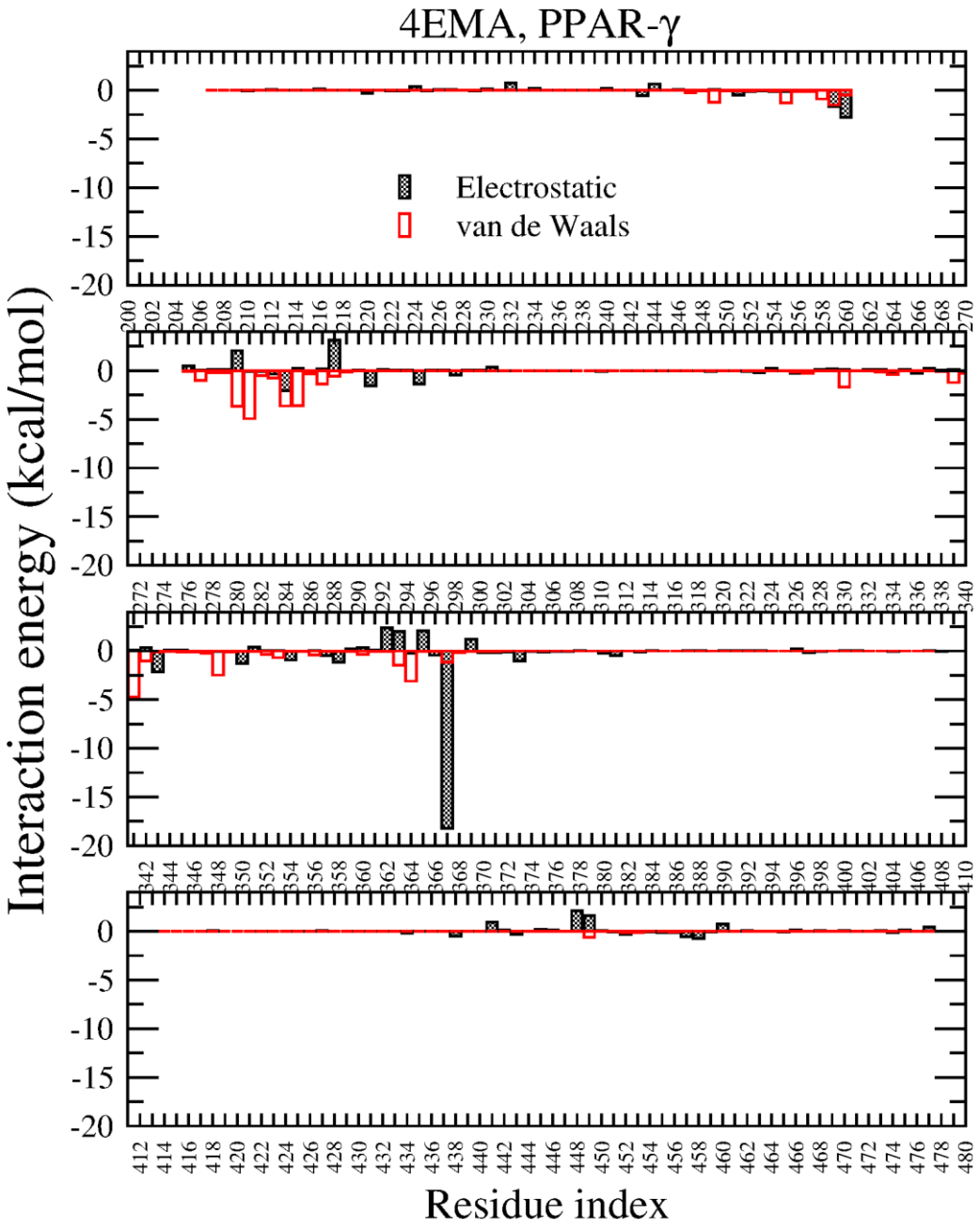

Figure S5. Per-residue interaction energies for PPAR-γ. Results were averaged over 4 MD runs.

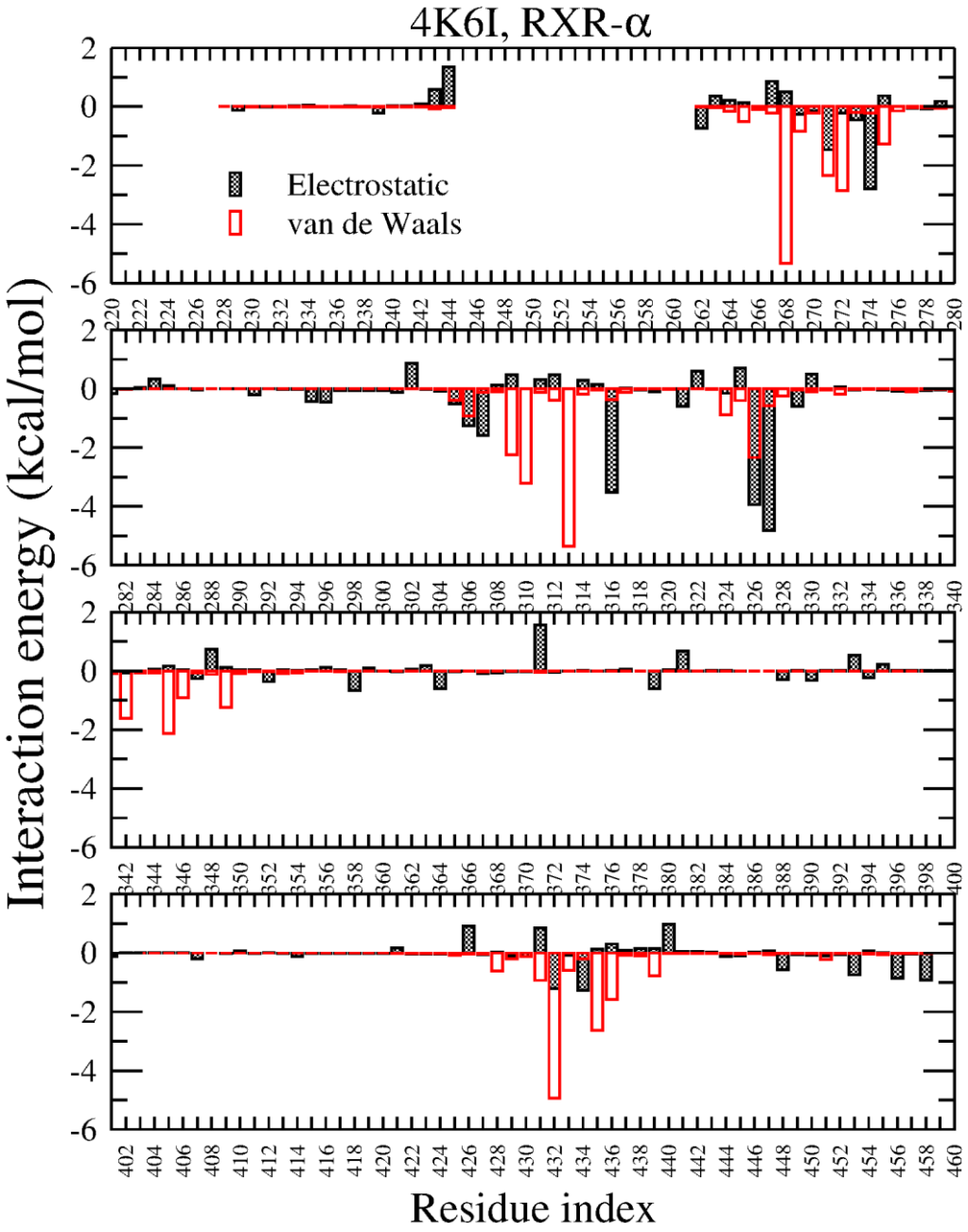

Figure S6. Per-residue interaction energies for RXR-α. Results were averaged over 4 MD runs.

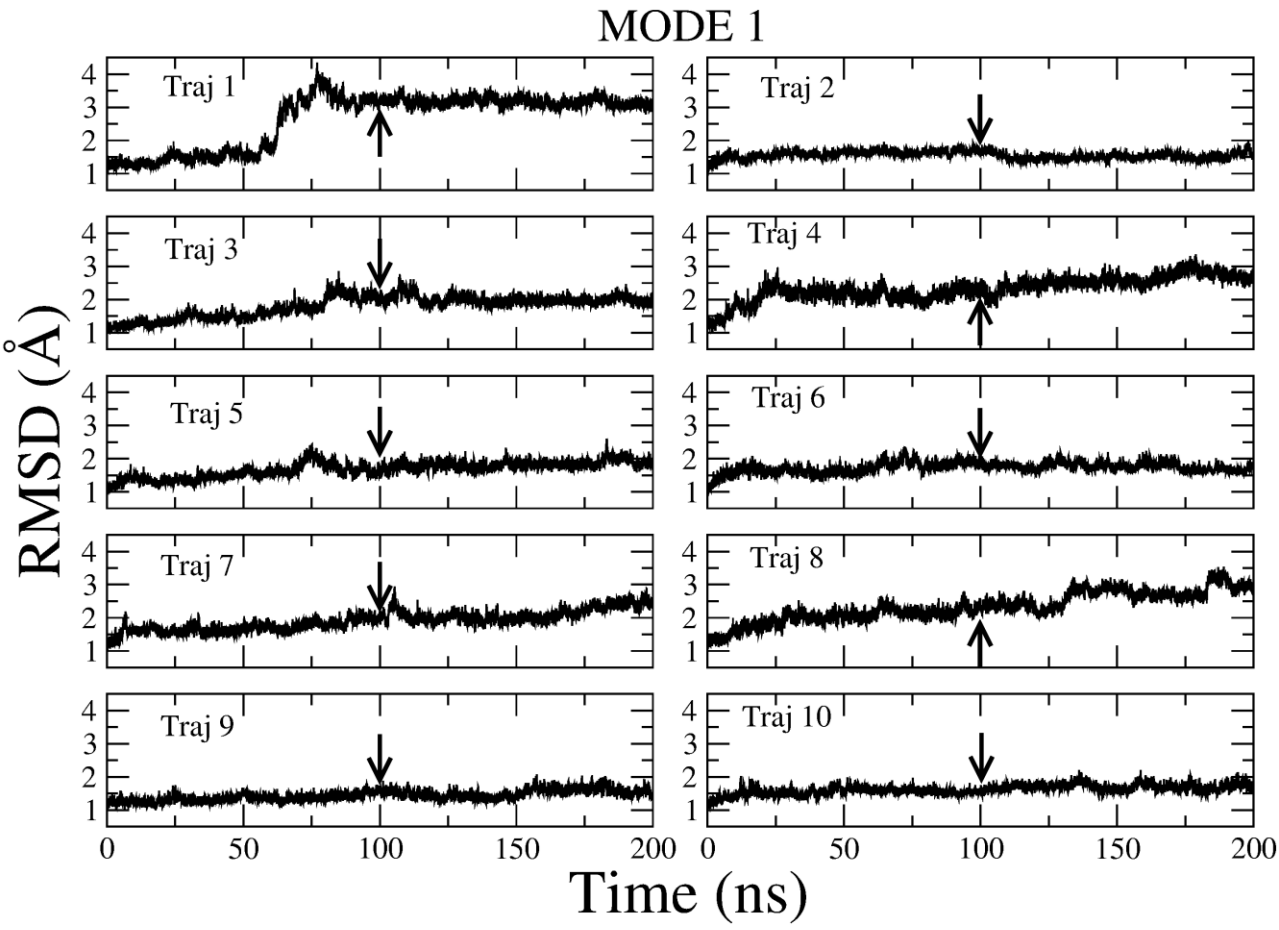

Figure S7: Time dependence of RMSD of β-secretase+bexarotene in the case where the MD simulation was performed using the configuration, obtained in Mode 1 (Fig. S2), as an initial configuration . The arrow indicates 100ns after which we have collected snapshots for estimating the binding free energy by the MM-PBSA method.

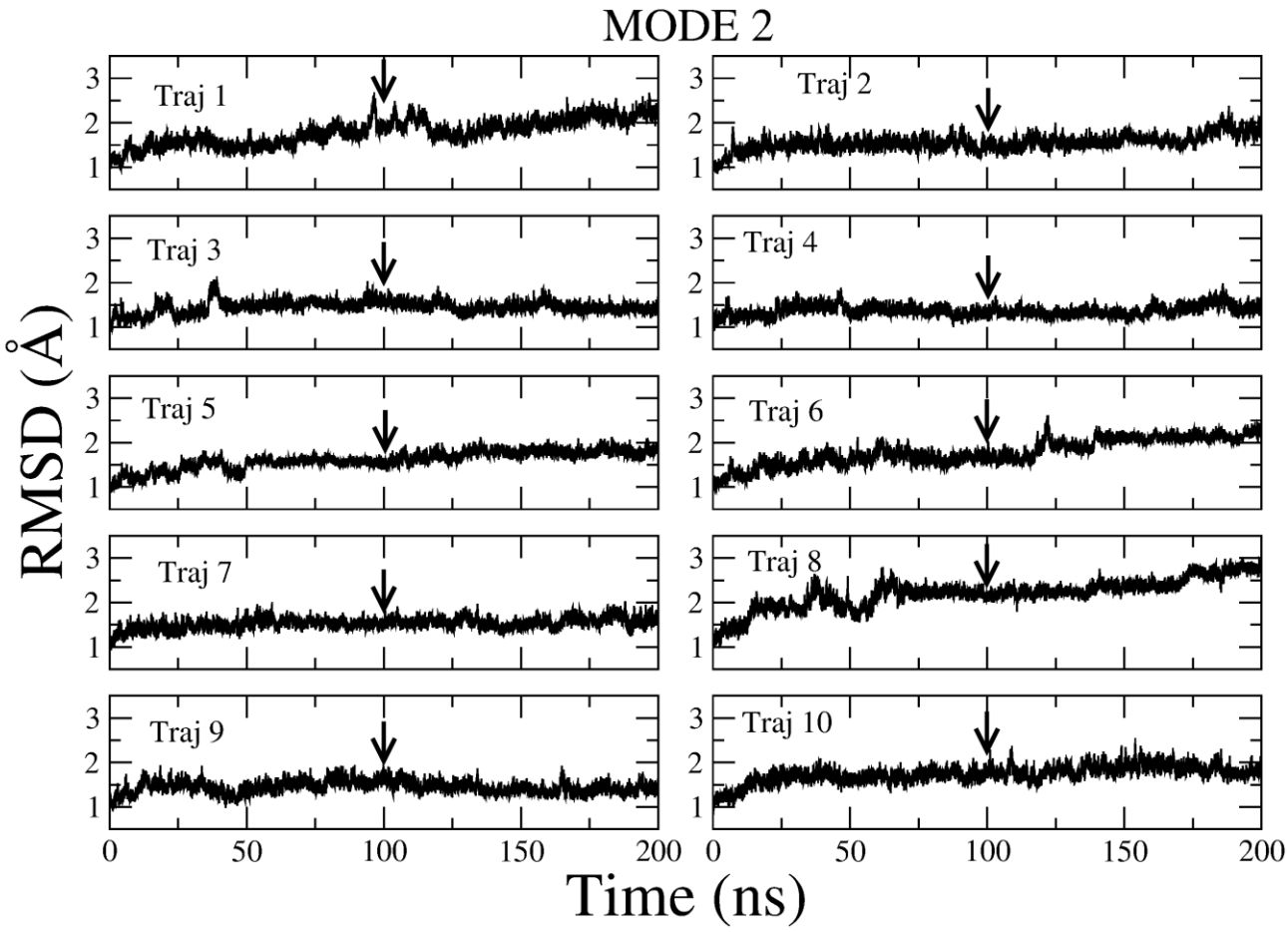

Figure S8: The same as in Figure S4 but for the case where the MD simulation was performed using the configuration, obtained in Mode 2 (Fig. S2), as an initial configuration.

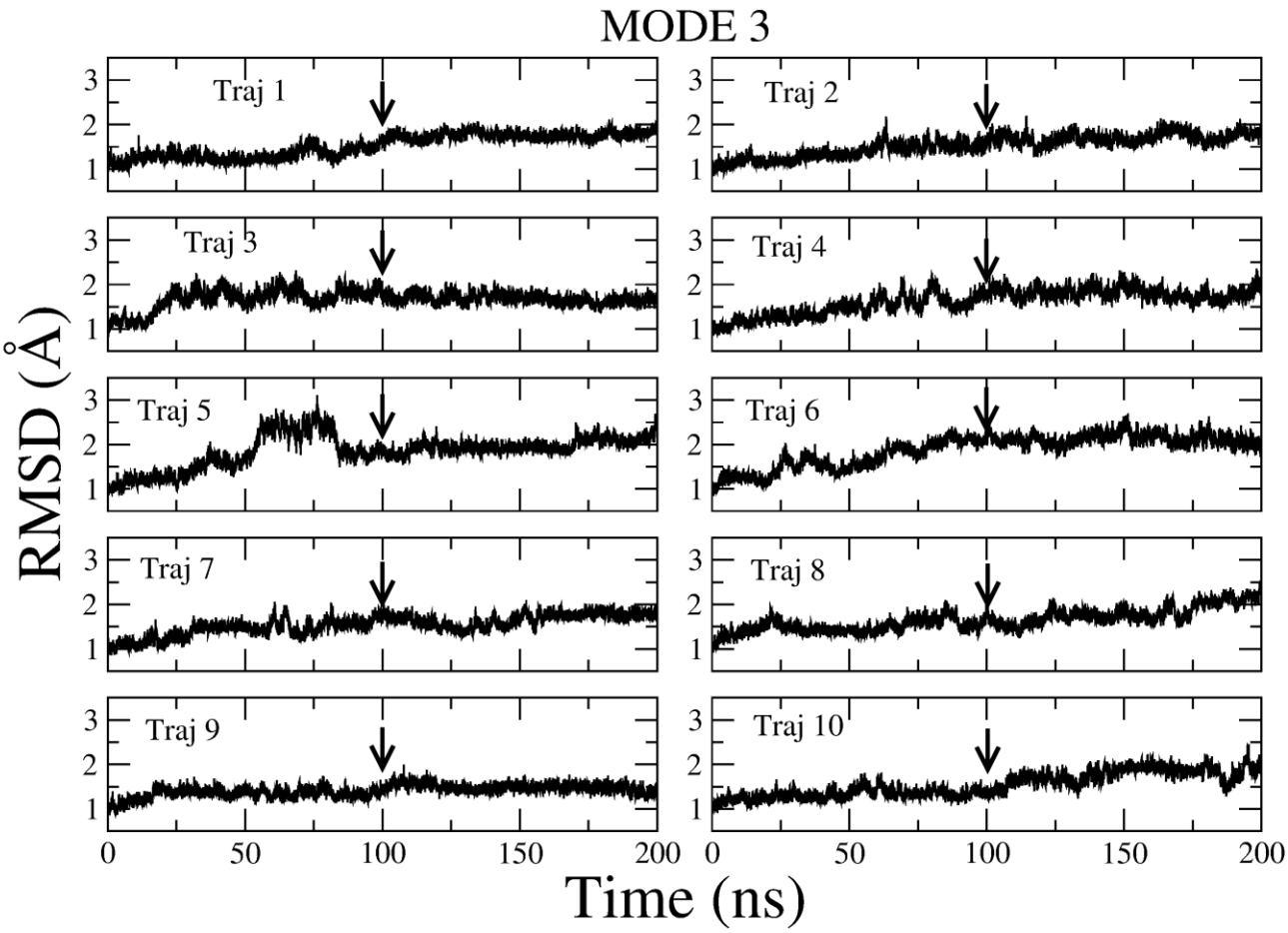

Figure S9: The same as in Figure S4 but for the case where the MD simulation was performed using the configuration, obtained in Mode 3 (Fig. S2), as an initial configuration.

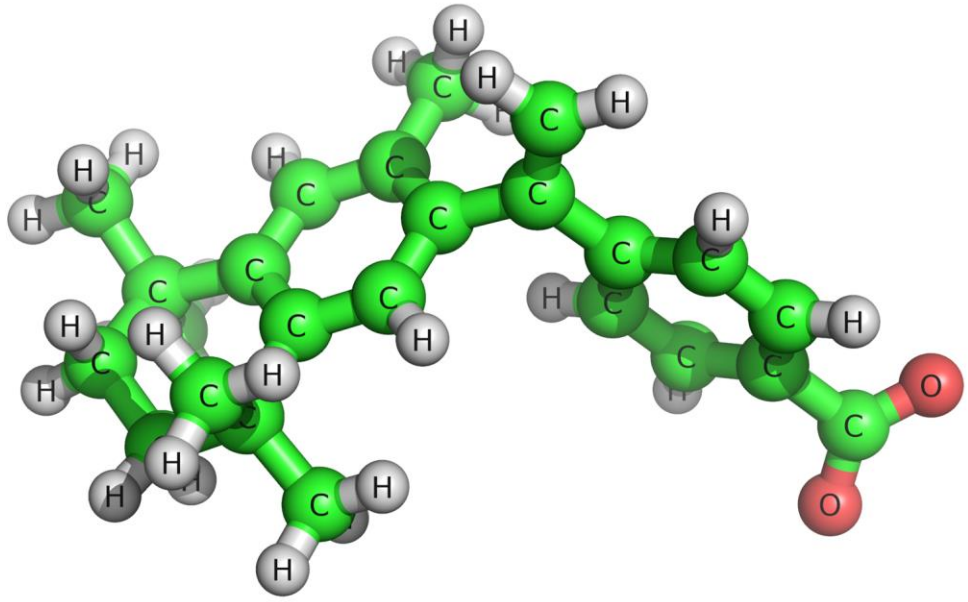

Figure S10: Three-dimensional structure of ionized bexarotene. The hydrogen atom from the carboxyl group is dissociated and bexarotene becomes negatively charged (-1).